Characteristics of solar flares associated with interplanetary shock or nonshock events at Earth

Xinhua Zhao,[1,2] Xueshang Feng,[1] and Chin-Chun Wu[3]

[1]   Solar flares and metric type II radio bursts are one kind of preliminary manifestations of solar disturbances and they are fundamental for predicting the arrival of associated interplanetary (IP) shocks at Earth. We statistically studied 347 solar flare type II radio burst events during 1997.2–2002.8 and found (1) only 37.5% of them were followed by the IP shocks at L1 (in other words, at Earth), the others without such IP shocks account for 62.5%; (2) the IP shocks associated with intense flares have large probability to arrive at Earth; (3) the IP shocks associated with central flares are more likely to arrive at Earth than those associated with the limb flares, and the most probable location for flares associated with IP shocks at Earth is $W20°$; and (4) there exists a east-west asymmetry in the distribution of geoeffectiveness of flare-associated IP shocks along the flare longitude. Most severe geomagnetic storms ($Dst_{\min} \leq -100$ nT) are usually caused by flare-associated shocks originating from western hemisphere or middle regions near central meridian, and the most probable location for strong flares associated with more intense geomagnetic storms is $W20°$ as well. These results could provide some criteria to estimate whether the associated shock would arrive at Earth and corresponding geomagnetic storm intensity.

1.   Introduction

[2]   It is well known that various kinds of solar transient activities such as solar flares, disappearing filaments and coronal mass ejections (CMEs) are responsible for strong IP disturbances and corresponding nonrecurrent geomagnetic disturbances. However, not all solar transient phenomena can arrive at Earth and cause geomagnetic disturbances. *Cane et al.* [2000] found that only about half of frontside halo CMEs during 1996–1999 encountered the Earth. *Park et al.* [2002] pointed out that only 35–45% of solar flares stronger than M1.0 were correlated with storm sudden commencements (SSC) on Earth. *Fry et al.* [2003] studied 173 solar flare type II radio events during 1997.2–2000.10 and discovered that only 62 of them were followed by IP shocks identified at L1 by ACE and/or WIND. *Yermolaev et al.* [2005] presented a comprehensive review of statistical analysis of the phenomena on the Sun, in IP space and in the Earth's magnetosphere, and found low probability of geoeffectiveness for solar disturbances (40–50%). *McKenna-Lawlor et al.* [2006] detected that only 59 of 173 solar flare type II radio burst events during 2000.11–

2002.8 were associated with the IP shocks at L1 by using a rigorous Rankine-Hugoniot analysis procedure. These results demonstrate that many solar disturbances do not hit the Earth and cause corresponding geoeffects because of their limited spatial extent and/or their propagation direction far away from the Sun-Earth line [*Cane et al.*, 2000]. Therefore forecasting of geomagnetic conditions based on observations of the solar phenomena may contain high level of false alarm [*Yermolaev et al.*, 2005].

[3]   Our purpose is trying to probe the characteristics of the solar disturbances with/without IP manifestations at Earth. It is really widely agreed that the IP shocks at distance of 1 AU are usually driven by interplanetary ejecta (ICMEs or MCs). CMEs and flares are closely correlated solar transient phenomena regarded as the solar source of these IP disturbances. Actually, the growing observations support the point that flares and CMEs are two phenomena in one process just as suggested by *Harrison* [1996]. Also, *Dryer* [1996] proposed more directly that flares did, in fact, play a fundamental role in producing CMEs and interplanetary shocks. Therefore we carry out this study in virtue of statistical comparison, and use solar flares as a proxy for our sampled solar transient phenomena because of the close relationship between flares and CMEs. This kind of investigation, we believe, would contribute to improve the reliability of predicting solar-terrestrial effects and reduce the probability of false alarms.

2.   Data Collection

[4]   We have collected 347 solar flare type II radio burst events during 1997.2–2002.8 from the studies of *Fry et al.*

[1]Solar-Interplanetary-Geomagnetic Weather Group, State Key Laboratory for Space Weather, Center for Space Science and Applied Research, Chinese Academy of Sciences, Beijing, China.
[2]College of Earth Sciences, Graduate University of the Chinese Academy of Sciences, Beijing, China.
[3]Center for Space Plasma and Aeronomic Research, University of Alabama in Huntsville, Huntsville, Alabama, USA.
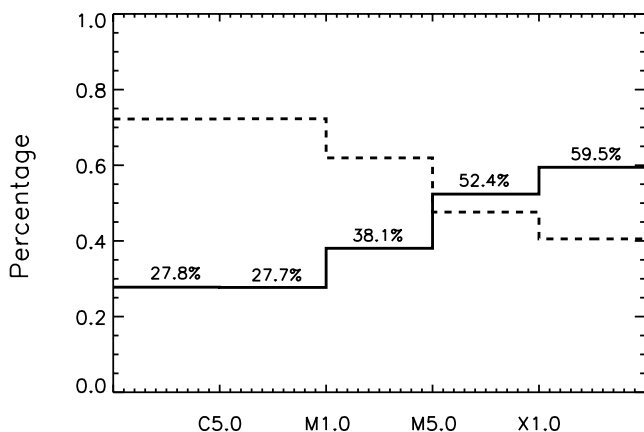
Figure 1. Percentage distribution for the events of type A (solid line) and type B (dashed line) at five flare intensity levels.

[2003] and *McKenna-Lawlor et al.* [2006]. They validated the correlative relation between the flares and their associated IP shocks at L1. For each event, the start time, flare location, coronal shock speed, flare intensity and arrival of the associated IP shock at L1 spacecraft are listed in these papers. The type II radio burst is interpreted as the signature of shock wave initiation in the solar corona and can be used to provide an estimation of initial shock speed. The flare intensity, defined by the maximum flux of X rays (of wavelength 0.1 to 0.8 nm, abbreviated as MFX) during the flaring process, is divided into five Classes, i.e., A (MFX of 10^{-5} erg/cm^2 s), B (MFX of 10^{-4} erg/cm^2 s), C (MFX of 10^{-3} erg/cm^2 s), M (MFX of 10^{-2} erg/cm^2 s), and X (MFX of 10^{-1} erg/cm^2 s). *Fry et al.* [2003] listed 173 events during 1997.2−2000.10, and *McKenna-Lawlor et al.* [2006] collected 207 events during the subsequent period of 2000.11−2002.8. The sum of their events covers a wide time range of nearly 5 years during the rising phase and solar maximum of Solar Cycle 23. Among these events, complete measurement data were not available for some events; also, ambiguity exists in the events where more than one solar flare were related to the same IP shock at L1. These questionable events are excluded from our samples for the validity of our study. Out of the 347 events in our sample, there are 130 shock events (130/347 = 37.5%) with presence of an associated IP shock observed at L1 spacecraft several days later, and we call these 130 events as type A. The remainder, 217 out of 347 (62.5%) no-shock events, i.e., without the associated IP shock observed at the near Earth space, are sorted out as type B. For events in type A, we selected the minimum *Dst* value, i.e., Dst_{min} in the interval of 48 hours following the arrival time of the IP shock at L1. As it is well known, the IP shocks, followed by regions of compressed magnetic field and enhanced plasma densities, usually cause geomagnetic disturbances via their interaction with the Earth's magnetosphere. If a time period longer than 48 hours was adopted, multiple shocks usually corresponded to the same *Dst* minimum and the direct causal relation between an individual shock and its corresponding Dst_{min} was less clear. This kind of postshock 48-hour rule has been previously

adopted by *Gonzalez and Tsurutani* [1987] and *Jurac et al.* [2002].

3. Analysis Results

3.1. Solar Flare Intensity

[5] Flare intensity of the total events, including both type A and type B, covers a wide range from class B, C, M, and X. We consider different event percentages of type A and type B along five intensity levels: (1) flare intensity below C5.0, i.e., 0 < MFX (erg/cm^2 s) ≤ 0.005; (2) intensity between C5.0-M1.0, i.e., 0.005 < MFX (erg/cm^2 s) ≤ 0.01; (3) intensity between M1.0−M5.0, i.e., 0.01 < MFX (erg/c m^2 s) ≤ 0.05; (4) intensity between M5.0 and X1.0, i.e., 0.05 < MFX (erg/cm^2 s) ≤ 0.1; and (5) intensity above X1.0, i.e., 0.1 < MFX (erg/cm^2 s) as shown in Figure 1. The solid and dashed line denote the percentages of type A and B, respectively, and their sum equals to 100% as defined. The percentages of type A events are labeled on the solid line as well. It can be seen from Figure 1 that the percentage of type A increases with the enhancement of flare intensity, while that of type B decreases. This means that the shocks associated with intense flares have more probability to arrive at Earth. *Smith and Dryer* [1990] found that the IP shock properties at 1 AU, such as strength, speed and angular extent, were primarily determined by the total energy release for the associated solar event by utilizing 2.5D MHD simulations. To some extent, the X-ray energy release in the 0.1 to 0.8 nm wavelength band used here can be considered as an indicator for the total energy released in the flaring process. The shocks associated with intense flares would possess large total energy and are likely to arrive at Earth before decaying into ordinary MHD waves.

3.2. Solar Flare Location

[6] Figure 2 gives the source location distribution for the events in type A (Figure 2a) and type B (Figure 2b). In latitude, flares are mainly distributed within ±40°; As for longitude (here refers to longitudinal distance from central meridian), the flares are broadly distributed. Limb events with source longitude near ±90°, even backside events with longitude greater than 90° or less than −90°, appeared in both type A and type B. For events with longitude greater than 100° or less than −100°, we draw them as diamonds in Figure 2a or triangles in Figure 2b near ±100° for compactness of the figure. There are some events originating near the limb in type A, which possibly indicates that IP shocks may evolve to have a broad shape in longitudinal direction when they propagate from the Sun to the Earth. On the other hand, the associated IP shocks were not detected at L1 following some flares close to central meridian. This shows the shock's propagation in IP space is a complicated process and many other factors would contribute to the shock's arrival at L1. Therefore, for an individual event, it is hard to predict whether the associated shock would reach the Earth only based on the relevant solar flare longitude.

[7] For further probing the contribution of flare locations, Figure 3a gives the event number percentage distribution along flare longitude. The solid line denotes the percentage of type A every 20° longitude, i.e., event number of type A within a certain 20° longitude interval divided by the total event number within this longitude interval. These percent-
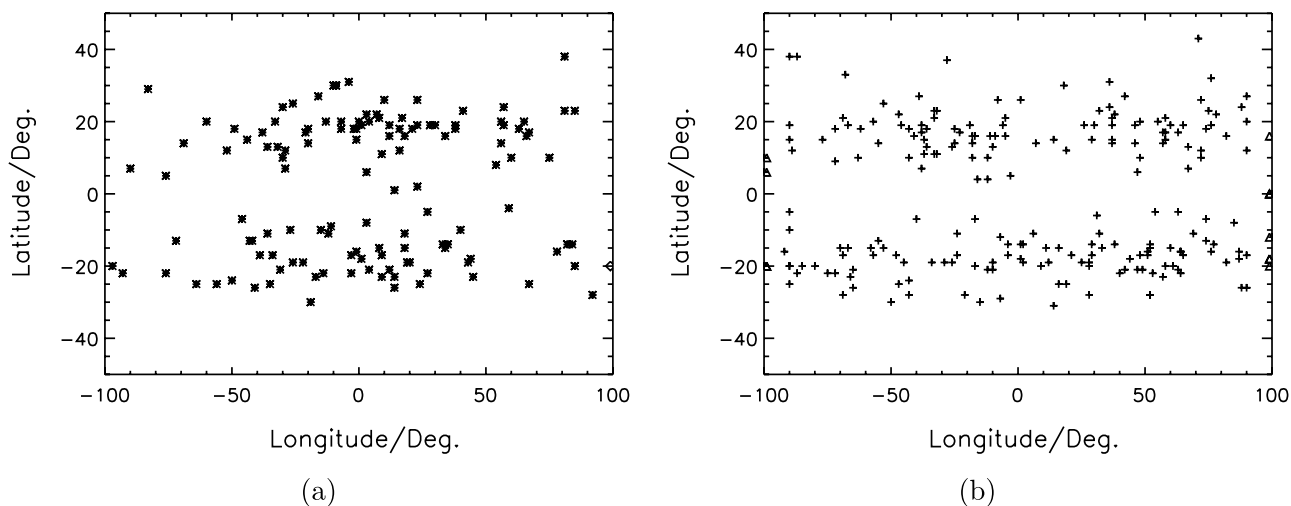
Figure 2. Distribution of flare location of (a) type A and (b) type B. Events with longitude $>100°$ or $<-100°$ are denoted by diamonds (Figure 2a) or triangles (Figure 2b) near $\pm100°$.

age values are labeled on the solid line. Similarly, the dashed line denotes the percentage of type B events. As the events with flare longitude out of $[E90°, W90°]$ are few, we do not compute the percentage in that longitude range. The percentage distributions along longitude are dramatically different for type A and B. For flares near the limb, the percentage of type A is low, while that of type B is high. As for flares near central meridian, more events belong to type A. This shows that the IP shocks associated with central flare are much easier to arrive at Earth than those associated with the limb flares. That is, the IP shocks associated with central flares would propagate just facing the Earth and are more likely to arrive. While the shocks associated with the limb flares would have large angle between their main direction and the Sun-Earth line, and would possibly miss the Earth. Another interesting finding is that the maximum (minimum) percentage of type A (B) is not at central meridian, but at $W20°$ as shown by the vertical line. The percentage of type A events (i.e., the flares followed by IP shocks at L1) at $W20°$ is 56.1%, much larger than the

percentage of 45.2% at symmetrical location of $E20°$. This westward offset of the source location, we believe, is reliable because it is found on a statistical study of a large number of included events. The reasons causing this solar source westward shift can be naturally owing to the interplanetary spiral magnetic field. *Wei et al.* [1985] and *Wei* [1987] studied the three-dimensional propagation of flare-associated IP shocks based on interplanetary scintillation (IPS) observations, and found that the fastest propagation direction of IP shocks tended to line along the spiral magnetic field in longitude. Recently, *Wang et al.* [2004] proposed a kinematic model to depict the deflection of CMEs in the interplanetary medium. In this model, a fast CME would be blocked by the background solar wind ahead and deflected to the east under the effect of the Parker spiral magnetic field. Supposing the interplanetary CMEs and their preceding IP shocks have similar general shape and propagation characteristics, then the propagation of IP shocks would also be effected by the spiral magnetic field. *Zhang et al.* [2003] also pointed out that the shock
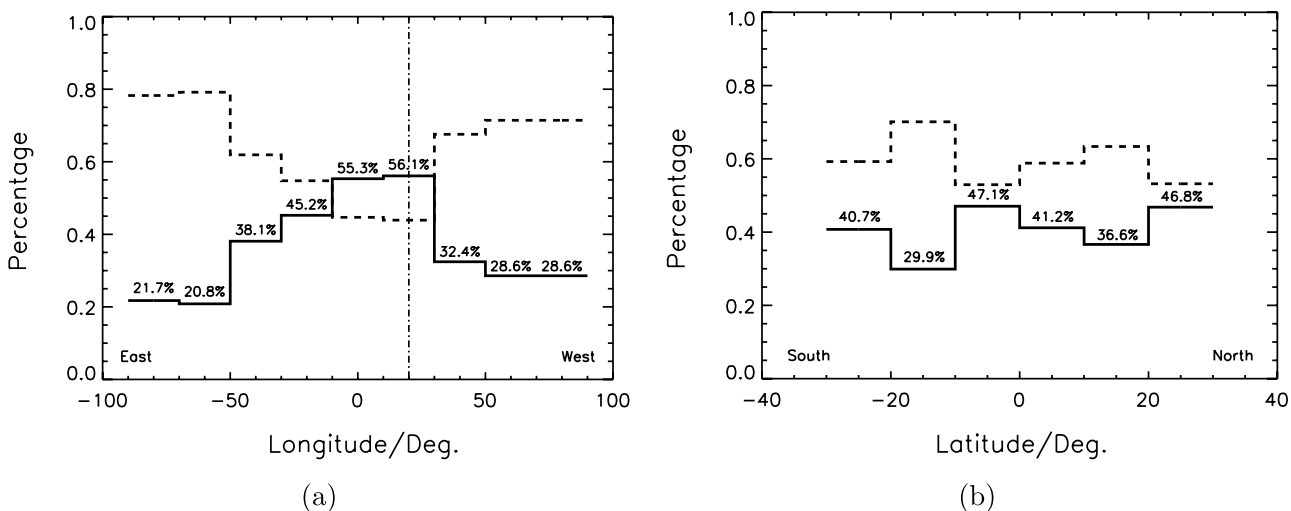

Figure 3. Percentage distribution along flare (a) longitude and (b) latitude for type A (solid line) and type B (dashed line).
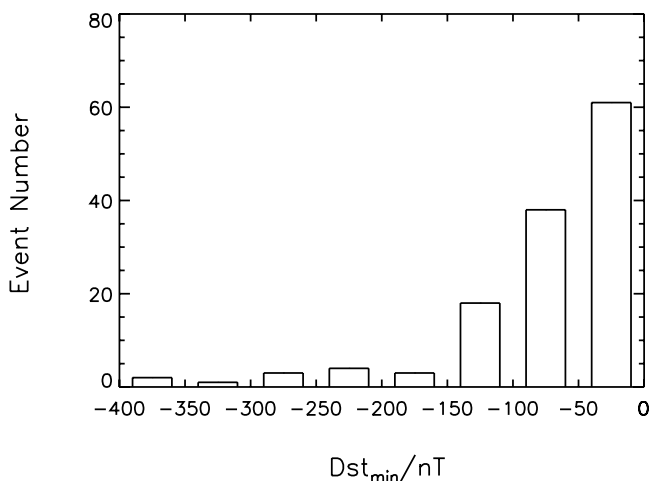
Figure 4. Histogram of Dst_{min} for the 130 shocks of type A.

accompanying an ICME originating from the western hemisphere may have a better chance to reach the Earth following the spiral field than that originating from the eastern hemisphere. However, how to quantitatively estimate this kind of effect is difficult and still needs further investigation.

[8] Figure 3b shows the percentage distribution along flare latitude. The solid and dashed lines represent the event number percentage of type A and type B, respectively (per $10°$ from $-30°$ to $30°$). In Figure 3b, the percentages vary rather randomly with small amplitudes with regard to latitude, and no maximum of percentage seems to appear anywhere. Therefore flare latitude, according to our statistics, has little correlation with the associated shock's probability of arrival at Earth.

3.3. Geoeffectiveness of Shocks

[9] Generally speaking, one of the most important factors that cause large geomagnetic storms is the Bs (southward Bz) component of the IMF in GSM coordinates. Such IMF changes can be caused by CMEs that are linked to solar flares or by helmet streamer and filament disruptions. They

may also be caused by high-speed/low-speed stream/stream interactions that could even strengthen into CIRs (corotating interaction regions). An interplanetary ejecta (such as an ICME with a magnetic cloud or other ejecta) containing a long lasting and strong Bs magnetic field component can cause a large storm event even if no preceding shock is driven by it. That is, the storm may be caused by the postshock Bs in the sheath region, within the magnetic cloud/ejecta, or by a combination of both [*Gonzalez et al.*, 1999; *Wu and Lepping*, 2002]. In this paper, we address only the flare-associated shock problem regardless of the various drivers that cause southward IMF. Among the 130 events in type A, 61 (47%) IP shocks were followed by weak geomagnetic disturbances with $0 > Dst_{min} > -50$ nT; The other 69 (53%) IP shocks were followed by moderate and intense geomagnetic storms with $Dst_{min} \leq -50$ nT. Figure 4 gives the histogram of Dst_{min} distribution for type A events. The geoeffective percentage of IP shocks of our result is consistent with previous studies [*Jurac et al.*, 2002; *Echer et al.*, 2004].

[10] For the 130 events in type A, Figure 5a gives the Dst minima plotted against the associated flare longitudes. An asymmetry distribution can be seen in Figure 5a. Although moderate geomagnetic storms (-100 nT $< Dst_{min} \leq -50$ nT) are caused by flare-associated shocks originating from both western and eastern hemisphere, the great geomagnetic storms ($Dst_{min} \leq -100$ nT) are usually caused by flare-associated shocks arising near central meridian or from western hemisphere. Wei and his coauthors [*Wei et al.*, 1985; *Wei*, 1987; *Wei and Deng*, 1987] are the first to address similar asymmetry in solar source longitude distribution, which are also found by *Wang et al.* [2002], *Cane and Richardson* [2003], and *Zhang et al.* [2003]. This kind of study suggests that the longitudinal asymmetrical distribution of solar sources may be a general feature. The solid line in Figure 5a represents the mean value of Dst_{min} in $20°$ bins from $-90°$ to $90°$ with computed error bars, and an asymmetry in the distribution of Dst_{min} mean value can be seen as well.

[11] Figure 5b shows these Dst minima versus the associated flare latitudes. The solid line represents the mean
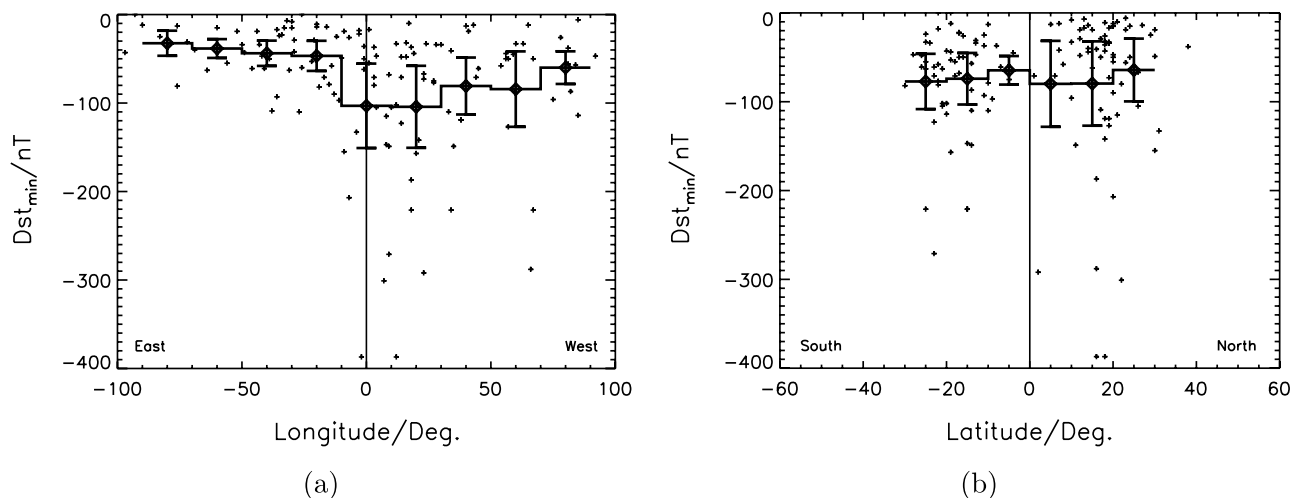

Figure 5. Dst_{min} plotted versus the associated flare (a) longitude and (b) latitude for the 130 shocks of type A. The mean values of Dst_{min} in certain longitude range with error bars are also shown.
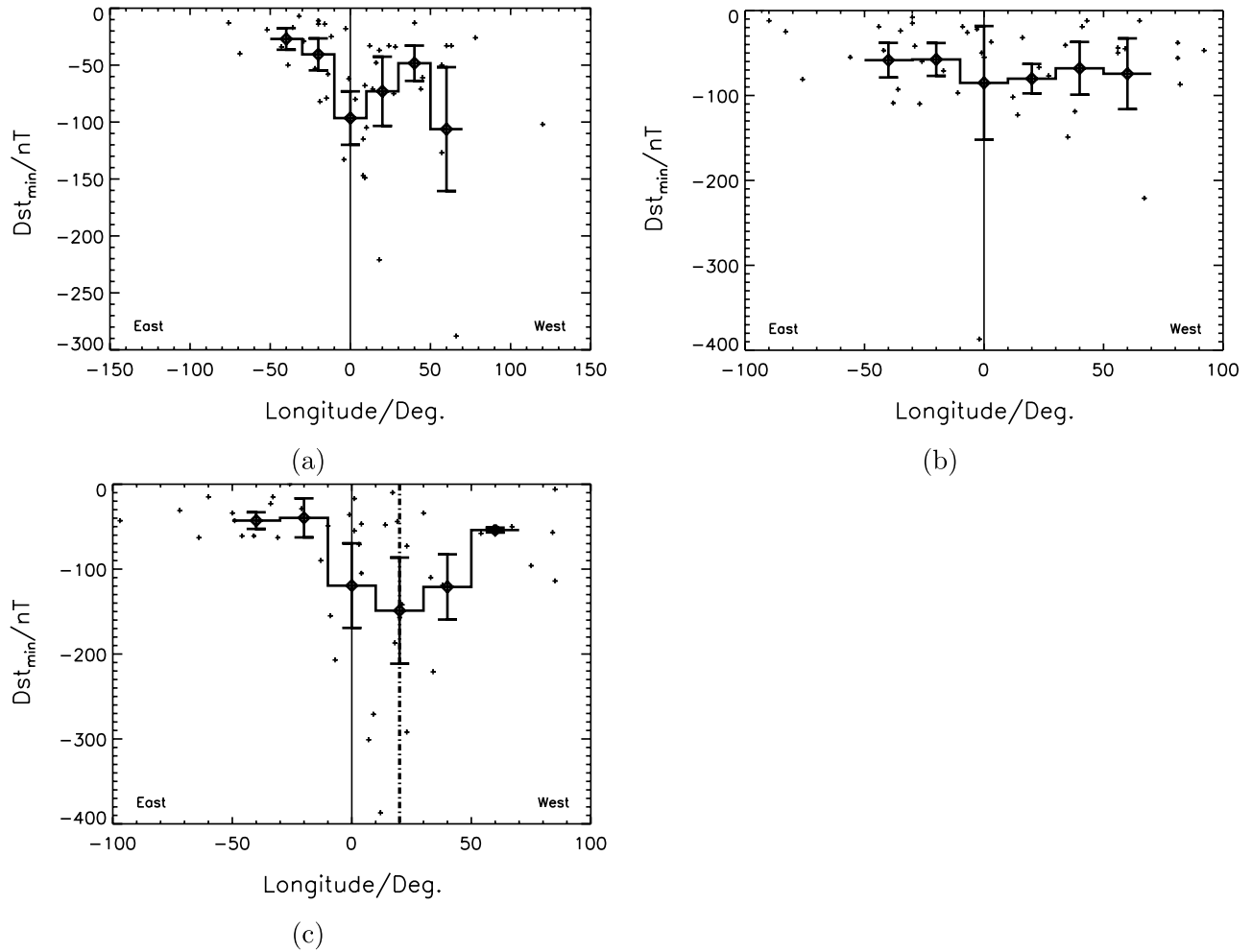
(a)

(b)

(c)

Figure 6. Geomagnetic storm intensity plotted versus the associated flare longitude for events of groups (a) I, (b) II, and (c) III. The mean values of Dst_{min} in 20° bins with error bars are also shown.

value of Dst_{min} in 10° bins from −30° to 30° with error bars computed. The distribution, fairly symmetrical about solar equator, indicates that the Dst_{min} has no evident dependence on the associated flare latitude.

[12] For further discussing the correlation between the associated flare longitude and corresponding Dst_{min}, we divide these 130 type A events into three groups: I. flare intensity below M1.0, i.e., $0 < $ MFX (erg/cm^2 s) ≤ 0.01; II. intensity between M1.0–M5.0, i.e., $0.01 < $ MFX (erg/cm^2 s) ≤ 0.05; and III. intensity above M5.0, i.e., $0.05 < $ MFX (erg/cm^2 s). The event numbers of these three groups are 43, 43 and 44, respectively, which are nearly equal. Figures 6a, 6b, and 6c give the Dst_{min} versus the associated flare longitude for these three groups, respectively. Solid lines represent the mean value of Dst_{min} in 20° bins. In Figure 6a, the event number of great geomagnetic storms with $Dst_{min} \leq -100$ nT is small; The distribution of Dst_{min} scatter randomly along flare longitude as it appears, and the mean value of Dst_{min} varies irregularly with regard to flare longitude. In Figure 6b, the distribution of Dst_{min} looks rather uniform, and the mean of Dst_{min} is nearly a constant. In these two cases, no preference of solar flare longitude could be found as far as its contribution to the related Dst_{min} is concerned. While for high-intensity solar flare events in

Figure 6c, the distribution of Dst_{min} along flare longitude is fairly well regulated. Though moderate and weak storms with $Dst_{min} > -100$ nT are scattered at large longitude range, great storms with $Dst_{min} \leq -100$ nT are restricted either near central meridian or at western hemisphere not far away from the center. The mean values of Dst_{min} in 20° bins show asymmetric distribution along longitude as well. The favored source location related to the most intense geomagnetic storms shifts from central meridian to $W20°$. This shift matches perfectly well with that in Figure 3a, where we consider the arrival of the associated shock at Earth. In conclusion, it can be seen that $W20°$ is a special important site, from which the flare-associated shocks would have better chance to arrive at Earth, and the corresponding geomagnetic storms would also tend to be more intense. This quantitative offset in solar source longitude is interesting and attractive even though it is only a coarse estimation. In spite of the fact that the event numbers are not large for the three cases after classification, our statistics are carried out in a restricted region of [−50°, 50°] that include the majority of the events. The mean value of Dst_{min} is a good index under this circumstance. The error bars of computing the Dst_{min} mean values are also shown in Figures 6a–6c. Therefore our statistical

results, we believe, are reasonable and acceptable. As for Figures 6a and 6b, the possible explanation may be: as the geomagnetic storm is the response of Earth's magnetosphere to solar wind conditions which involves many intricate physical processes, the influences of other factors on the storm intensity would exceed the influence of solar source longitude for weaker strength solar disturbance events (weaker solar flares in this case), so that such kind of longitude-depending property of Dst_{min} is obscured and fainted. Of course, much work needs to be done by using a larger sample of events to make sure the validity of our results.

4. Summary and Discussion

[13] Here a total subset of 347 flare events during 1997.2–2002.8 is used to statistically study the characteristics of solar flares associated with IP shock or nonshock events at L1. The preliminary conclusions of the present paper are as follows. The shocks associated with intense or central flares are more likely to arrive at Earth than those associated with weak or limb flares. The most probable location for flares associated with L1 IP shocks is $W20°$, but without any obvious latitude dependence. By coincidence, the most probable place for strong flares related to more intense geomagnetic storm is also $W20°$. For 130 events with IP shocks at L1, their geoeffectiveness has the east-west longitudinal asymmetry. Our statistical study also shows that the great geomagnetic storms ($Dst_{min} \leq -100$ nT) are usually caused by flare-associated shocks arising near central meridian or from western hemisphere. These new findings can be useful for predicting shock arrival and corresponding geomagnetic storm intensity.

References

Cane, H. V., and I. G. Richardson (2003), Interplanetary coronal mass ejections in the near-Earth solar wind during 1996–2002, *J. Geophys. Res.*, *108*(A4), 1156, doi:10.1029/2002JA009817.

Cane, H. V., I. G. Richardson, and O. C. St. Cyr (2000), Coronal mass ejections, interplanetary ejecta and geomagnetic storms, *Geophys. Res. Lett.*, *27*(21), 3591.

Dryer, M. (1996), Comments on the origins of coronal mass ejections, *Sol. Phys.*, *169*, 421.

Echer, E., M. V. Alves, and W. D. Gonzalez (2004), Geoeffectiveness of interplanetary shocks during solar minimum (1995–1996) and solar maximum (2000), *Sol. Phys.*, *221*, 361.

Fry, C. D., M. Dryer, Z. Smith, W. Sun, C. S. Deehr, and S.-I. Akasofu (2003), Forecasting solar wind structures and shock arrival times using an ensemble of models, *J. Geophys. Res.*, *108*(A2), 1070, doi:10.1029/2002JA009474.

Gonzalez, W. D., and B. T. Tsurutani (1987), Criteria of interplanetary parameters causing intense magnetic storms (Dst < −100nT), *Planet. Space Sci.*, *35*(9), 1101.

Gonzalez, W. D., B. T. Tsurutani, and A. L. Clua de Gonzalez (1999), Interplanetary origin of geomagnetic storms, *Space Sci. Rev.*, *88*, 529.

Harrison, R. A. (1996), Coronal magnetic storms: A new perspective on flares and the 'solar flare myth' debate, *Sol. Phys.*, *166*(2), 441.

Jurac, S., J. C. Kasper, J. D. Richardson, and A. J. Lazarus (2002), Geomagnetic disturbances and their relationship to interplanetary shock parameters, *Geophys. Res. Lett.*, *29*(10), 1463, doi:10.1029/2001GL014034.

McKenna-Lawlor, S. M. P., M. Dryer, M. D. Kartalev, Z. Smith, C. D. Fry, W. Sun, C. S. Deehr, K. Kecskemety, and K. Kudela (2006), Near real-time predictions of the arrival at Earth of flare-generated shocks during Solar Cycle 23, *J. Geophys. Res.*, doi:10.1029/2005JA011162, in press.

Park, Y. D., Y.-J. Moon, S. Iraida Kim, and H. S. Yun (2002), Delay times between geoeffective solar disturbances and geomagnetic indices, *Astrophys. Space Sci.*, *279*, 343.

Smith, Z., and M. Dryer (1990), MHD study of temporal and spatial evolution of simulated interplanetary shocks in the ecliptic plane within 1 AU, *Sol. Phys.*, *129*, 387.

Wang, Y. M., P. Z. Ye, S. Wang, G. P. Zhou, and J. X. Wang (2002), A statistical study on the geoeffectiveness of Earth-directed coronal mass ejections from March 1997 to December 2000, *J. Geophys. Res.*, *107*(A11), 1340, doi:10.1029/2002JA009244.

Wang, Y. M., C. L. Shen, S. Wang, and P. Z. Ye (2004), Deflection of coronal mass ejection in the interplanetary medium, *Sol. Phys.*, *222*, 329.

Wei, F. S. (1987), Statistical study on the asymmetrical propagation of flare-shocks, *Sci. China A*, *2*, 186.

Wei, F. S., and X. D. Deng (1987), North-south asymmetrical propagation of flare-shocks, *Chin. J. Geophys.*, *30*(5), 443.

Wei, F. S., G. Yang, and G. L. Zhang (1985), Three-dimensional propagation characteristics of flare-shocks based on IPS observations, *Acta Astrophys. Sin.*, *5*(3), 214.

Wu, C.-C., and R. P. Lepping (2002), Effects of magnetic clouds on the occurrence of geomagnetic storms: The first 4 years of Wind, *J. Geophys. Res.*, *107*(A10), 1314, doi:10.1029/2001JA000161.

Yermolaev, Y. I., M. Y. Yermolaev, G. N. Zastenker, L. M. Zelenyi, A. A. Petrukovich, and J.-A. Sauvaud (2005), Statistical studies of geomagnetic storm dependencies on solar and interplanetary events: A review, *Planet. Space Sci.*, *53*, 189.

Zhang, J., K. P. Dere, R. A. Howard, and V. Bothmer (2003), Identification of solar sources of major geomagnetic storms between 1996 and 2000, *Astrophys. J.*, *582*, 520.

—————————

X. Feng and X. Zhao, SIGMA Weather Group, State Key Laboratory for Space Weather, Center for Space Science and Applied Research, Chinese Academy of Sciences, P.O. Box 8701, Beijing 100080, China. (fengx@spaceweather.ac.cn; xhzhao@spaceweather.ac.cn)

C.-C. Wu, CSPAR, University of Alabama in Huntsville, Huntsville, AL 35899, USA.